Mar Biol (2012) 159:1621–1631
DOI 10.1007/s00227-012-1920-y

METHOD

Imaging of surface O_2 dynamics in corals with magnetic micro optode particles

J. Fabricius-Dyg · G. Mistlberger · M. Staal · S. M. Borisov · I. Klimant · M. Kühl

Received: 30 June 2011 / Accepted: 7 March 2012 / Published online: 24 March 2012
© Springer-Verlag 2012

Abstract We present a new method for quantifying spatio-temporal O_2 distribution and dynamics at biologically active surfaces with a complex surface topography. Magnetized O_2 optode microparticles (~80–100 μm) containing the NIR-emitting luminophore platinum (II) meso-tetra (4-fluorophenyl) tetrabenzoporphyrin (PtTPTBPF; ex. max. 615 nm; em. max. 780 nm) were distributed across the surface tissue of the scleractinian coral *Caulastrea furcata* and were held in place with a strong magnet. The O_2-dependent luminescence of the particles was mapped with a lifetime imaging system enabling measurements of the lateral surface heterogeneity of the O_2 microenvironment across coral polyps exposed to flow. Mapping steady-state O_2 concentrations under constant light and O_2 dynamics during experimental light–dark shifts enabled us to identify zones of different photosynthetic activities within a single coral polyp linked to the distribution of coral host pigments. Measurements under increasing irradiance showed typical saturation curves of O_2 concentration and estimates of gross photosynthesis that could be spatially resolved at ~100 μm pixel resolution. The new method for O_2 imaging with magnetized optode particles has much potential to be used in studies of the surface microenvironment of other aquatic systems such as sediments, biofilms, plant, and animal tissue.

Communicated by M. Huettel.

J. Fabricius-Dyg · M. Staal · M. Kühl (✉)
Marine Biology Section, Department of Biology, University of Copenhagen, Strandpromenaden 5, 3000 Helsingør, Denmark
e-mail: mkuhl@bio.ku.dk

G. Mistlberger · S. M. Borisov · I. Klimant
Institute of Analytical Chemistry and Food Chemistry, Graz University of Technology, Stremayrgasse 9, 8010 Graz, Austria

M. Kühl
Plant Functional Biology and Climate Change Cluster, University of Technology Sydney, PO Box 123, Ultimo, NSW 2007, Australia

M. Kühl
Singapore Centre on Environmental Life Sciences Engineering, School of Biological Sciences, Nanyang Technological University, 60 Nanyang Drive, SBS-01n-42, 637551 Singapore, Singapore

Introduction

The concentration of O_2 is a key environmental variable in ecological and physiological studies of aquatic organisms and systems, where it is a measure of the net outcome of photosynthesis, respiration, and biogeochemical mineralization processes (Klimant et al. 1997; Fenchel and Finlay 2008; Glud 2008). In corals, O_2 levels are modulated by (1) the photosynthetic O_2 production of microalgal endosymbionts in the host tissue, (2) the combined respiration of the animal host and its symbionts, and (3) the transport of O_2 via advection and diffusion. The chemical conditions in coral tissue vary dynamically from hyperoxic conditions in the light to hypoxia in darkness (Kühl et al. 1995). Such dynamics also exhibits spatial variability due to differences in symbiont density and host pigmentations as well as inter- and intra-colonial variability in symbiont light acclimation (Ulstrup et al. 2006) and the balance between photosynthesis and respiration (Cooper et al. 2011). The balance of these processes is responsive to environmental stress leading to deleterious effects such as temperature-induced coral bleaching, disease, and tissue injury (e.g., Andersen et al. 2010; Ulstrup et al. 2007). Thus, the

chemical landscape in terms of O_2 distribution in corals is modulated by changes in coral physiology, tissue organization, and environmental conditions. Such links between structure and function are largely unexplored and require experimental methods enabling fine scale mapping of O_2 conditions in relation to the coral tissue and skeleton structures.

Electrochemical and optical microsensors (Revsbech 2005; Kühl 2005) can measure O_2 with high spatio-temporal resolution yielding detailed insight to microenvironmental controls of photosynthesis and respiration in corals (Kühl et al. 1995; de Beer et al. 2000), foraminifera (Köhler-Rink and Kühl 2005), and biofilms (Kühl et al. 1996). However, such microsensor measurements are *de facto* point measurements that are difficult, if not impossible, to extrapolate to larger scales in complex and heterogeneous systems. Earlier attempts to map the chemical heterogeneity in corals have involved microsensor point measurement of O_2 and temperature profiles in transects across coral polyps (e.g., de Beer et al. 2000; Jimenez et al. 2008, 2011) in experiments lasting several hours.

Alternatively, O_2 can be spatially mapped with imaging technology in combination with luminescent O_2 indicators immobilized on planar sensor foils (reviewed in Kühl and Polerecky 2008). The measuring principle of such O_2 optodes is based on the dynamic collisional quenching of a luminescent indicator dye by molecular oxygen. When the indicator is excited by photons, it will emit red-shifted photons to return to its ground state with a given time constant, that is, the luminescence decay or lifetime. In the presence of O_2, the excited indicator can transfer its energy upon collision with molecular oxygen, which is intermittently changed to a singlet state. Singlet oxygen is rapidly converted back into O_2, mainly through non-radiative deactivation via heat emission, and no net consumption of O_2 is caused by the optical measurement (Klimant et al. 1997; Bacon and Demas 1987). The net result of the energy transfer to O_2 is a reduction in indicator luminescence intensity, I, and a decrease in the luminescence lifetime, τ.

Immobilization of O_2 indicators in polymers often leads to a non-ideal quenching behavior, and the relation between luminescence and O_2 concentration is often described by a modified Stern–Volmer equation (Carraway et al. 1991; Klimant et al. 1997):

$$\frac{\tau}{\tau_0} = \frac{I}{I_0} = \left(\frac{\alpha}{(1 + K_{sv} \cdot [O_2])} \right) + (1 - \alpha) \quad (1)$$

where I_0 and τ_0 are the luminescence intensity and lifetime under anoxia, I and τ are the luminescence intensity and lifetime for a given O_2 concentration, α is the fraction of quenchable dye, and K_{sv} is the Stern–Volmer quenching constant, which quantifies the efficiency of the quenching and therefore the sensitivity of the sensor (Klimant et al. 1997).

First, O_2 imaging studies used simple luminescence intensity imaging of planar optodes (Glud et al. 1996) but now luminescence lifetime imaging is commonly used (Kühl and Polerecky 2008); the lifetime measuring principle is described in Holst et al. (1998) and Holst and Grunwald (2001). Such sensors have, for example, been used for respiration and photosynthesis studies in microbial communities (e.g., Glud et al. 1996, 1999), studies of O_2 dynamics in coral skeleton (Kühl et al. 2008), and in studies of the effects of infauna and fish on sediment O_2 conditions (Wenzhöfer and Glud 2004; Behrens et al. 2007). However, use of planar sensor foils requires fitting the investigated system tightly to the sensor surface, for example, by insertion of the planar optode into sediment for measuring vertical O_2 gradients (Glud et al. 1996, 2001) or by growing biofilms directly on top of the sensor foil (Kühl et al. 2007; Staal et al. 2011). The presence of a planar optode in the diffusive boundary layer (DBL) above corals would create its own boundary layer, and even the presence of a thin microsensor tip in proximity of the coral tissue can induce a local erosion of the DBL (Glud et al. 1995).

Luminescent O_2 indicators can be immobilized into nm- or μm-sized particles (e.g., Borisov and Klimant 2008a, b), which preserve the measuring properties of macro optodes and can be distributed or fixed over a complex surface. Embedding the indicator in particles is important because singlet oxygen is formed during the O_2-sensing mechanism, which can affect biology if dissolved O_2 indicators are used in solution (Dobrucki 2001). When the indicator is immobilized in a polymer matrix in a planar optode or a microparticle, such exposure is minimized, as singlet oxygen dissipates faster than it can diffuse out of the sensor layer/particle. The use of sensor microparticles for distributed O_2 sensing is thus chemically non-invasive. In this study, we present a new method using such microparticles for mapping spatial O_2 distribution and dynamics at the tissue surface across single coral polyps exposed to flow and defined irradiance levels. The scope is to present the new method, its advantages, and its current limitations rather than a fully replicated physiological study of corals. The new method is also well suited for mapping O_2 in applications within many other areas of experimental biology.

Materials and methods

Sensor materials

We used the newly developed O_2 indicator platinum (II) meso-tetra(4-fluorophenyl) tetrabenzoporphyrin (PtTPTBPF). The synthesis of this luminophore and its photophysical properties are described in detail elsewhere (Borisov et al.

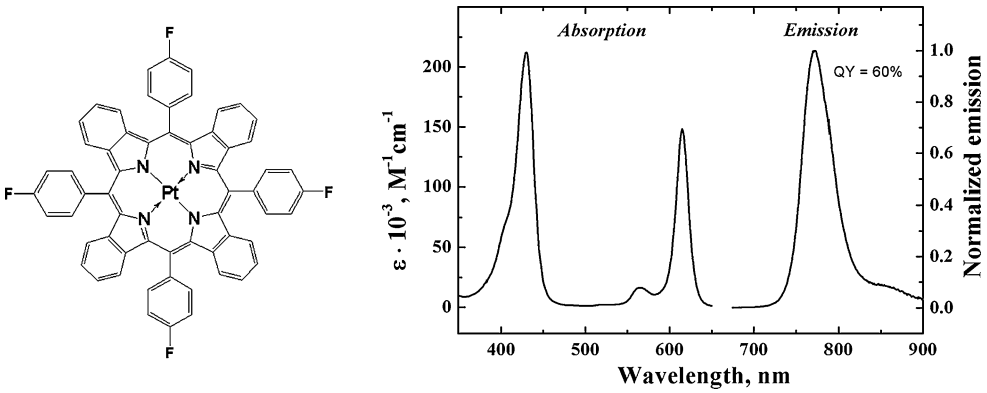

Fig. 1 Chemical structure (*left*) and spectral absorption and emission properties of the luminescent O_2 indicator platinum (II) meso-tetra (4-fluorophenyl) tetrabenzoporphyrin (PtTPTBPF) (*right*)

2008a, b, 2009). PtTPTBPF has a higher brightness (defined as the product of the molar absorption coefficient, ε, and the emission quantum yield) and a higher photostability as compared to other platinum(II) and palladium(II) benzoporphyrin complexes (Borisov et al. 2009). An advantageous feature of PtTPTBPF is the possibility to excite the indicator with low energetic red light (ex. max. ~615 nm) and to monitor the O_2-dependent luminescence in the NIR region (em. max. ~780 nm) (Fig. 1), that is, well outside the fluorescence range of, for example, chlorophyll or GFP-like host pigments (Oswald et al. 2007).

Temperature influences both the decay time of PtTPTBPF under anoxic conditions (which decreases due to thermal quenching) and the Stern–Volmer quenching constant K_{sv} (which increases with temperature) (Borisov et al. 2008a, b). The decay time of PtTPTBPF in the particles is only minor affected by temperature (about 0.07 %/°K). The effect of temperature on K_{sv} is more significant (about 1.3 %/K). In other words, alteration of temperature by 1 °C would produce an error of ~1.3 % in determination of O_2 partial pressure.

Preparation of O_2-sensitive microparticles

PtTPTBPF was immobilized into a copolymer of polystyrene and maleic acid anhydride (PS-MA, 11 % of maleic anhydride). Optodes made with this copolymer matrix have a similar sensitivity to O_2 as polystyrene-based optodes, but cast copolymer films can easily be ground to microparticles, and the microparticles are rendered water-dispersible due to the hydrophilic surface provided by the carboxyl groups of the maleic acid. Use of low molecular weight PS-MA (14,000 Da) is best for this purpose, since copolymers with a higher MW are more difficult to grind mechanically.

A weight of 15 mg of PtTPTBPF (prepared according to Borisov et al. 2009) and 1 g of PS-MA (EF-80, kindly provided by Sartomer Inc; http://www.sartomereurope.com) were dissolved in 3 g of chloroform. The solution was evaporated in a Petri dish, and the resulting bulk material was ground in an agate mortar. The particles were dispersed in a mixture of 20 mL ethanol and 1 mL 1 M NaOH and were stirred with a magnetic stirring bar for 24 h. The beads were washed 5 times with ethanol and 3 times with water to remove indicator dye absorbed on the particle surface. The obtained aqueous suspension (1.5 % w/w) was stored at 4 °C. Magnetic O_2 sensing microparticles were prepared using a similar procedure, but 300 mg of lipophilic magnetite nanoparticles (prepared according to Mistlberger et al. 2010b) and 50 mg of titanium dioxide nanoparticles (P 170, Kemira Inc.; http://www.kemira.com) were additionally added to the solution of indicator and polymer in chloroform prior to evaporation and grinding.

A 1.5 % w/w particle stock solution was diluted 10 times before application to corals via a pipette. First experiments showed that deposited non-magnetic particles were mostly transported away from corals subject to flow. However, microparticles with magnetite could be immobilized onto the coral surface tissue by help of a strong magnet placed under the coral (see below). We did not observe any significant flow or sedimentation-driven particle redistribution of magnetic particles. Therefore, only magnetized microparticles were used in actual coral experiments.

Imaging system

We used a modular luminescence lifetime imaging system (Holst et al. 1998; Holst and Grunwald 2001) consisting of a sensitive fast gate-able camera with a 1,280 × 1,028 (2/3″) CCD-Interline Progressive Scan chip (PCO Sensimod, PCO GmbH, Germany), which acquires images of luminescence intensity during defined time intervals relative to the excitation of the O_2 indicator with light emitting diodes (LEDs). Custom-made software (LookMolli vers. 1.8.5; Holst and Grunwald 2001) controlled the timing of image acquisition and LEDs. In our study, the CCD camera was equipped with a macro lens (Xenoplan XNP 1.4/17, Schneider-Kreutznach, Germany) resulting in a resolution of ~35 µm per pixel at a focal distance of ~7 cm over a

field of view of ~3.5 cm × 4.5 cm. The lens was equipped with a RG9 emission long pass filter ($\lambda > 720$ nm, Schott GmbH). Two high power red LEDs with a Lambertian beam pattern (1 W, LXHL-MD1D, em. max. 625 nm, Luxeon) were mounted close to the lens in an adjustable holder for homogeneous illumination of the sampled region. The LEDs were equipped with collimating lenses to intensify excitation over the central focus area of ~2 cm^2 in the cameras field of view

Luminescence lifetime images were determined from acquisition of luminescence intensity images over two different time windows, w1 and w2, after the eclipse of the excitation light (Holst et al. 1998):

$$\tau = \frac{\Delta t}{\ln\left(\frac{I_{w1}}{I_{w2}}\right)} \quad (2)$$

The time intervals are defined by several system settings: Δ_{ex} is the time interval where the LEDs are turned on for excitation; Δ_1 is the delay time before start of w1, which can be used to avoid natural bioluminescence with a much faster decay time than the O_2 indicator; Δ_{Int} sets the time duration that the CCD chip uses to records values for w1 and w2; Δ_2 sets the time interval between stop exposure of w1 and start exposure of w2 image. This measuring scheme is repeated numerous times within a preset integration time of the CCD camera determining the total number of measuring cycles for each data set acquisition. The integration time enables signal amplification improving the signal to noise ratio. In our study, we used the following setting: $\Delta_{ex} = 10$ µs, $\Delta_1 = 1$ µs, $\Delta_2 = 3$ µs, and $\Delta_{Int} = 3$ µs; these values were chosen after optimization tests with the O_2 indicator particles showing optimal pixel values relative to the system noise.

Experimental setup

The imaging system was mounted vertically above a flow chamber placed on top of an aquarium tank (inner dimensions: 41.5 × 25 × 24 cm) with artificial seawater (HW Meersalz Professional, Wiegand GmbH, Germany; $S = 38$) kept at 25.5 °C by help of an aquarium heater (Fig. 2). The water was aerated with an aquarium air pump keeping the O_2 concentration in the seawater at atmospheric saturation under the experimental salinity and temperature (205 µmol L^{-1}; Ramsing and Gundersen 2000). A submersible water pump circulated the water through the flow chamber (inner dimensions: 8 × 25 × 7 cm) at flow velocity of ~0.5 cm s^{-1}. Light driving photosynthesis was supplied from a fiber-optic halogen lamp (KL2500, Schott GmbH, Germany) equipped with a glass filter blocking wavelengths >720 nm (CalFlex X, Balzers, Switzerland) and a collimating lens. In comparison to sunlight, the color temperature of halogen lamps is lower and contains much less blue wavelengths. Incident light at the surface of the coral was measured as downwelling quantum irradiance (PAR, 400–700 nm) for different lamp settings using a quantum irradiance meter (LI-192, LI-250, LiCor Inc., USA).

Experiments were done with single polyps (~1–1.5 cm wide and 2–3 cm high) of the scleractinian coral *Caulastrea furcata* mounted with waterproof putty onto a small plastic base. The corals were grown under an irradiance of ~100 µmol photons m^{-2} s^{-1} in a large tank of artificial aerated seawater (25.7 °C). Prior to experiments, individual coral polyps were carefully transferred to the flow chamber avoiding air exposure. The polyp was mounted in a custom-made Perspex device (Fig. 2b) directly on top of a neodymium magnet (circular flat shape, height: 0.9 cm, radius: 0.9 cm, Chen Yang Technologies GmbH, Germany), which created a strong magnetic field over the polyp surface. The 10× diluted solution of magnetic sensor particles was kept in an Eppendorf tube, which was thoroughly mixed before application. Aliquots of 30 µL were applied very slowly over the coral tissue using a 100 µL pipette, until a homogenous distribution of the particles was achieved.

Coral polyps are able to expand or contract their tissue and secrete mucus in response to external stimuli and/or stress. In our study, abrupt changes in light conditions as well as transfer from the growth tank to the experimental setup stimulated the corals to slowly expand their mouth disk and the area around it initiating mucus secretion. Thereby, particles could be moved in excreted mucus treads rearranging the sensor particles. While mucus secretion and rearrangement of the beads could not be prevented completely, it was largely avoided by allowing the coral to acclimate for ~1 h after transfer to the experimental setup before application of the magnetic beads.

Calibration

A heating/cooler circulator (Julabo F25-HD, Germany) was connected to the thermostating loop of a custom-built aluminum calibration chamber, which was maintained at a constant temperature of 25.5 °C. The chamber was designed as a gas tight flow trough cell with an inlet, an outlet, and a transparent removable lid. A droplet of a 10× diluted solution of a 1.5 % w/w PS-MA magnetic sensor bead suspension was placed on a thin neodymium magnet in the calibration chamber. The inlet of the calibration chamber was connected with gastight Tygon tubing to a PC-controlled gas mixer (Sensor Sense GM-1, The Netherlands) that generated a constant gas stream through the chamber. To prevent evaporation from the droplet with the sensor particles, the gas was flushed through water in a

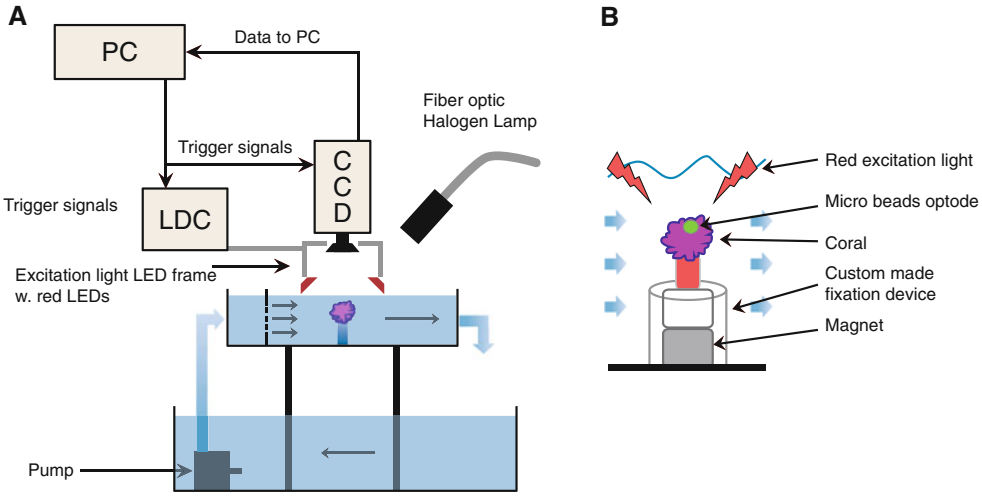

Fig. 2 Schematic drawing of experimental set-up for imaging O_2 concentration over coral tissue (**a**), and a custom-built magnet holder enabling immobilization of magnetic O_2 optode microparticles onto the tissue surface of a coral sample (**b**)

humidifier vial prior to entering the calibration chamber. We used a total gas flow rate of 0.4 l min^{-1} and programmed the gas mixer to provide a defined range of gas mixtures with 11 linear stepwise increases in O_2 concentration going from 0 to 40 % O_2 saturation. Each concentration step was kept for 5 min to guarantee steady-state O_2 conditions for each calibration measurement.

Mapping of O_2 dynamics across coral tissue surface

After application of the magnetic O_2 sensor particles, the coral was illuminated for ~5–10 min to attain steady-state O_2 conditions at the coral surface (Kühl et al. 1995) before the lamp was switched off and image acquisition started. Sixty sequential measurements per irradiance were collected. Three such series were measured at the same irradiance but with image acquisition of 10, 20, and 30 s intervals, respectively. The first O_2 image in these series was taken as representative for the steady-state O_2 concentration at the tissue surface.

Prior to imaging fast O_2 dynamics, the coral was kept in the dark ~10 min until constant lifetime values were obtained, that is, steady-state O_2 conditions. Subsequently, the coral was illuminated for 5 min with each of the following irradiances: 63, 149, 309, 596, and 1,229 µmol photons m^{-2} s^{-1}. After each irradiance period, the light was switched off and the camera system was set to record 60 image sets with a 3-s interval between successive images. In principle, the average O_2 concentration depletion rate over the first few images (3–4 depending on noise levels) after onset of darkness estimates the gross photosynthesis rate of the coral assuming (1) steady-state O_2 conditions before darkening, (2) an unchanged O_2 consumption rate just before and after darkening, and (3) no significant changes in the spatial O_2 concentration gradients (Glud et al. 1999).

Image analysis and calculations

Image sequences were imported into ImageJ (Vers. 1.42Q; http://rsbweb.nih.gov/jj) as a w1 stack and a w2 image stack, respectively. Luminescence lifetimes, τ, were calculated according to Eq. 2, where Δt (6 µs) was the time interval between start exposure of w1 to start exposure of w2. Subsequently, τ_0/τ was calculated, using the τ_0 value (48.4 µs) found in our calibration at 0 % O_2. The ratio stack was then further processed using the obtained calibration curve. Multiplication with a mask created from a thresholded w1 image sequence removed the pixels that did not contain magnetic beads. The resulting image stacks described the spatio-temporal O_2 dynamics.

Proxies of gross photosynthesis rate were calculated from the rate of change in O_2 concentration in the first seconds after darkening in two ways: (A) For calculations at pixel level, we duplicated the O_2 concentration image stack, removed the last image in one stack and the first image in the other stack. By subtracting these two image stacks, we thus obtained a stack of O_2 concentration changes, $\Delta[O_2]$, between image n and image $n + 1$. By dividing this $\Delta[O_2]$ stack with the time interval between images, we obtained a stack of O_2 depletion rate images. Using the z-projection function of ImageJ, we used this stack to calculate an average O_2 depletion rate image as a proxy for gross photosynthesis rate. (B) Alternatively, we used thresholded sequences of O_2 concentration images, where regions of interest (ROI) could be set (using the ImageJ plug in "Time Series Analyzer"; http://rsbweb.nih.gov/ij/plugins/time-series.html), in which values from each image in the time sequence were averaged, so that each time point was only represented by the average values of the ROI. The initial part of such data sets was fitted with a linear trend line, the slope of which yielded a proxy for gross photosynthesis.

Results

Calibration

The O_2-dependent luminescence lifetime, τ, of the magnetic microparticles varied over a range of almost 40 µs for the range of O_2 concentrations used in our calibration (Fig. 3a), with a luminescence lifetime under anoxia, τ_0, of 48.4 µs. Note that the luminescence intensity or lifetime decreased non-linearly with increasing O_2 concentration. Largest relative signal changes were thus found at the lowest O_2 concentration range, while the absolute signal changes became less and less with increasing O_2 concentration, ultimately defining the upper detection limit. In the present study, the operational range of the O_2-sensitive microparticles was 0 to ~400 µmol O_2 L^{-1}. The relative standard error of the individual calibration points was constant, showing a variability in the microparticle luminescence of ~10 % at a given O_2 concentration, which may in part be attributable to the fact that the microparticle size was larger than the camera pixel resolution.

The magnetic O_2 sensor particles exhibited a slightly non-linear Stern–Volmer plot of the calibration data (Fig. 3b), where fitting of Eq. 1 yielded a small non-quenchable fraction, that is, $(1\text{-}\alpha) = 0.036$, and a K_{sv} of 0.1229 (% O_2)$^{-1}$.

For a given batch of magnetic sensor particles, we obtained similar calibration curves when comparing calibrations done at time intervals over weeks up to several months—with the beads stored in a refrigerator in between. The maximum O_2 concentration at which the beads can be used is approximately 900–1,000 µmol O_2 L^{-1}. At higher concentrations, the fluorescence signal to noise levels became too low. In the image calculations, we used a threshold minimum pixel value of 30, that is, 4–5 times the background pixel value, which was ~5–10. Pixel values below this threshold were excluded from the analysis. Consequently, the accuracy of O_2 pictures is somewhat lower at low pixel values, which is reflected in an increased standard deviation and a lower peak height (data not shown). It was found that the absolute standard deviation increased from ~12 µM under hypoxic conditions up to ~55 µM at an O_2 concentration of 400 µM in the calibration images.

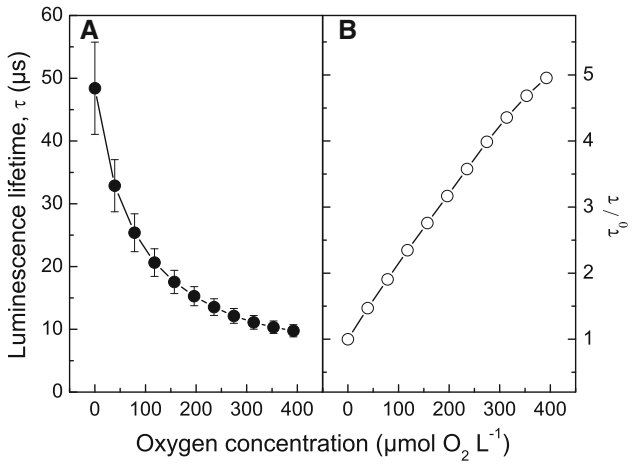

Fig. 3 Calibration curve of magnetic O_2 optode microparticles. **a** Luminescence lifetime, τ, versus O_2 concentration. *Symbols* represent average ± SE. **b** A Stern–Volmer plot of τ_0/τ versus O_2 concentration

Mapping of O_2 concentration dynamics

First measurements with the magnetic sensor particles clearly showed their potential to resolve the lateral heterogeneity in O_2 concentration over the upper tissue surface of corals (Fig. 4). The luminescence lifetime imaging approach used here allows quantification of O_2 independent on the absolute luminescence intensity, which is affected, for example, by uneven illumination or distribution of the sensor particles. It was possible to superimpose images of the coral structure with O_2 concentration images enabling mapping of O_2 concentration to specific structures of the coral polyp such as, for example, the mouth disk with tissue containing fluorescent host pigments and the surrounding coenosarc tissue.

Under increasing irradiance, the average tissue surface O_2 concentrations expressed a typical saturation curve (Fig. 5a–g). Histograms of all pixel values of O_2 concentrations over the coral tissue showed a normal distribution that became wider at increasing irradiance, indicative of increasing differences in surface O_2 concentration over the tissue (Fig. 5h). The O_2 dynamics at the coral tissue surface during experimental light–dark shifts showed differences between tissue types (Fig. 6). A region representative of the surrounding coenosarc tissue exhibited higher O_2 concentrations in saturating light (404 µmol O_2 L^{-1}) and a lower concentration in the dark (84 µmol O_2 L^{-1}) than a region representative of the mouth tissue (313 µmol O_2 L^{-1} in light and 144 µmol O_2 L^{-1} in the dark, respectively).

The spatial distribution of gross photosynthetic activity over the coral tissue under increasing irradiance was mapped from O_2 concentration images acquired immediately after darkening (Fig. 7). Pixel–pixel rate calculations yielded a rather noisy picture due to inherent variability in pixel levels for a given O_2 concentration (Fig. 3). Calculations of photosynthesis from the O_2 depletion rate within specific ROI yielded relative standard errors within a region of interest were 20–27 %. Comparison of the different tissue types indicated that photosynthetic activity was higher in the coenosarc tissue as compared to the mouth disk tissue containing coral host pigments (Fig. 7).

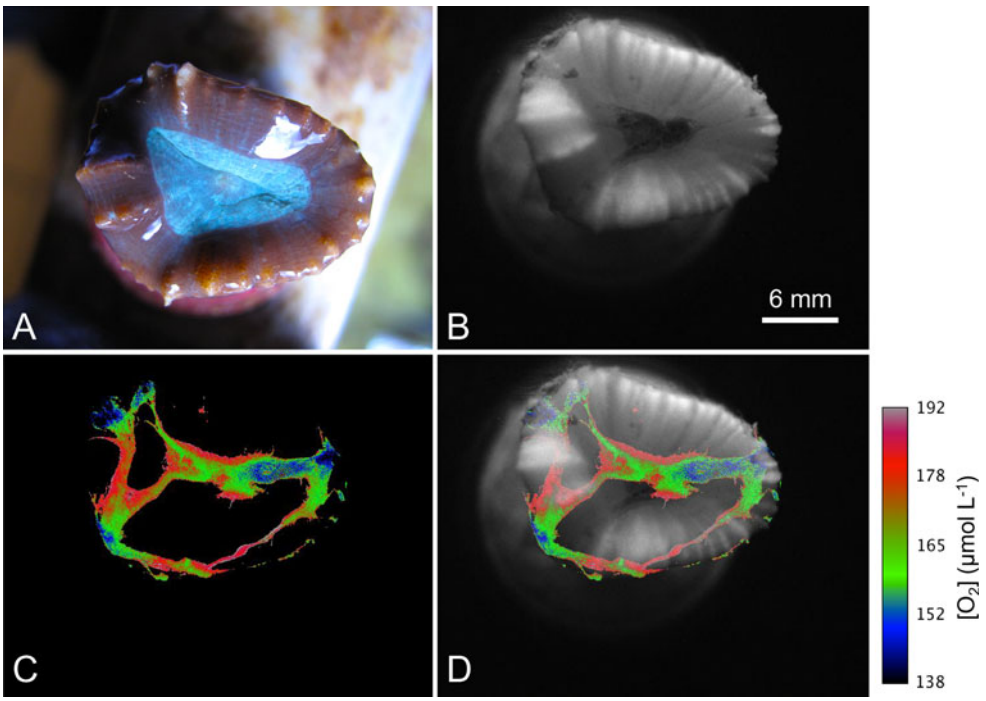

Fig. 4 Images of a single polyp of the coral *Caulastrea furcata* showing (**a**) a *color* photograph of the polyp with the presence of fluorescent host pigments in the *bluish-green* polyp tissue surrounding the mouth disk and the *brown* coenosarcs tissue, (**b**) a luminescence intensity picture of the polyp, (**c**) an image of the spatial O_2 distribution over the polyp surface under an irradiance of 63 µmol photons m^{-2} s^{-1}, and (**d**) an overlay of the polyp structure and the O_2 concentration image. The O_2 concentration in the air-saturated overlaying water was 205 µmol L^{-1}

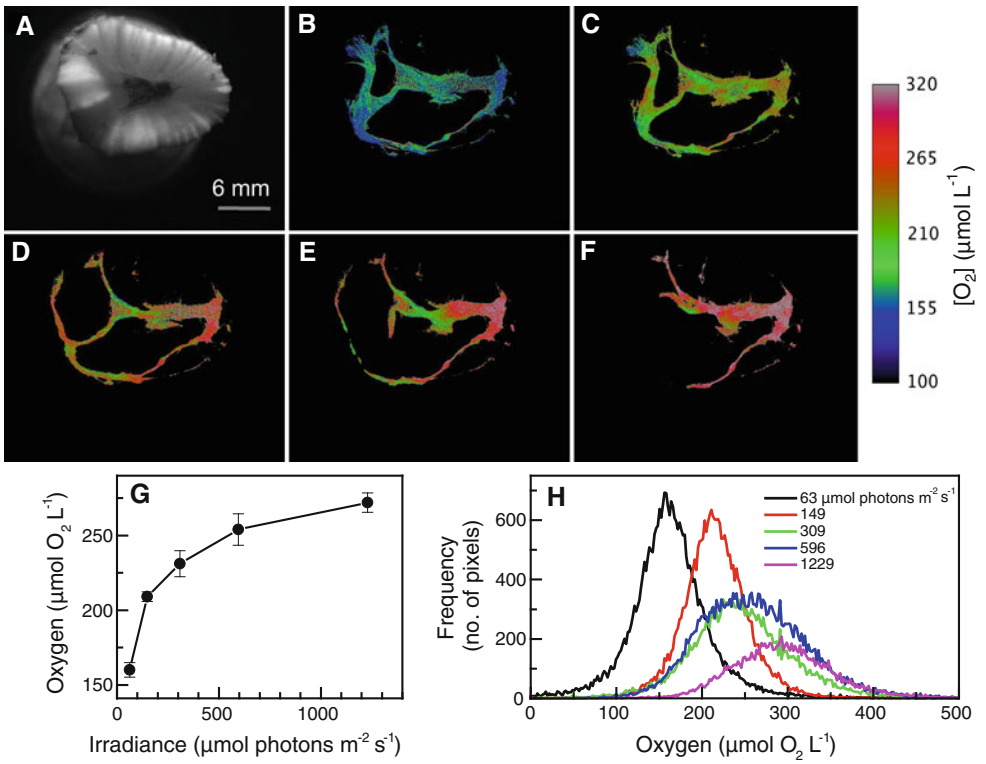

Fig. 5 Imaging of steady-state O_2 concentration at the tissue surface of the coral *Caulastrea furcata* as a function of an increasing irradiance. **a** Reference picture of luminescence intensity. **b–f** Images of O_2 concentration at increasing irradiance: 63, 149, 309, 596, and 1,229 µmol photons m^{-2} s^{-1}. **g** The development of the average O_2 concentration in each image as a function of irradiance. *Symbols* represent average ± SE (n = 18,220 pixels). **h** Frequency of O_2 concentration values in image **b–f**. The *scale bar* applies to **b–f**. The O_2 concentration in the air-saturated overlaying water was 205 µmol L^{-1}

Discussion

The use of distributed magnetized O_2 optode microparticles is a new method enabling the mapping of O_2 concentration and dynamics over complex coral tissue surfaces. The magnetic sensor particles can be easily fabricated in larger quantities using a simple protocol. If prolonged storage times are required, the beads can also be freeze-dried and re-dispersed whenever necessary. In this first presentation of the technique, we were able to image

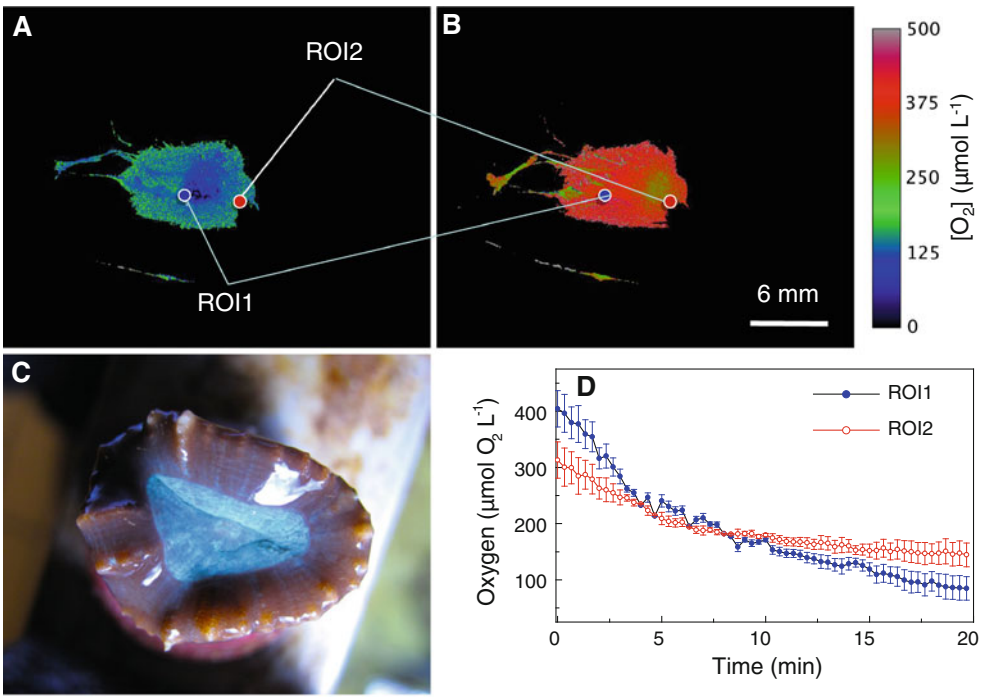

Fig. 6 Spatio-temporal O_2 concentration dynamics measured over 20 min in polyp tissue around the mouth disk (ROI 1) and coenosarc tissue (ROI 2). **a**, **b** Steady-state O_2 concentration images measured in darkness and under an irradiance of 63 µmol photons m^{-2} s^{-1}, respectively. **c** Digital photo of the coral polyp. **d** O_2 depletion in ROI 1 and 2 (average ± SE, $n = 22{,}800$ pixels) over 20 min after darkening. The O_2 concentration in the air-saturated overlaying water was 205 µmol L^{-1}

O_2 concentration and estimates of photosynthetic activity within a single coral polyp. We could assign differences in O_2 dynamics under increasing irradiance to different coral tissue types, that is, coenosarc tissue and polyp tissue around the mouth disk containing fluorescent host pigments that may affect light availability and act as photo protective agents (Salih et al. 2000). Earlier studies of intra polyp differences in O_2 concentration and photosynthetic production have been limited to relatively few O_2 microsensor point measurements (e.g., Kühl et al. 1995; Ulstrup et al. 2006). The possibility to superimpose images of O_2 distribution and dynamics onto structural images of the coral, thereby linking the chemical O_2 landscape and photosynthetic activity distribution to coral morphology, is thus a major step forward in our ability to resolve microenvironmental controls and responses of coral ecophysiology.

However, application of the new microparticle methodology on corals also faces special challenges due to coral secretion of mucus under stress. In our study, we could avoid or minimize this by allowing corals to acclimate to experimental conditions in the flow chamber after transfer from the growth tank. However, there was still some mucus production in parts of the coral, which hindered more permanent deposition of sensor particles in these regions. Although we applied a relatively dilute suspension of particles, we cannot rule out that the presence of sensor particles on the coral tissue induced such mucus secretion, as corals can be stressed by sediment deposition (Weber et al. 2006). More studies of such a potential interference need to be done.

Intense mucus production could also keep sensor particles at a distance to the tissue surface, which would cause less dynamics in O_2 concentration and underestimation of photosynthetic activity, and this may be the reason behind our relative low GRP rates (Fig. 7) as compared to other studies (e.g., Kühl et al. 1995). In this study, we used relatively large (~80–100 µm) magnetized particles with a slow response time of several seconds, as judged from O_2 dynamics in highly active biofilms, showing strong O_2 depletion within 5 s after a light–dark shift at saturating irradiance (Staal et al. unpublished data). This is a limitation in connection with gross photosynthesis measurements via rapid light–dark shifts, as slow response limits the spatial resolution due to diffusive "smearing" of true concentration differences and dynamics (Glud et al. 1999). Future studies should resolve this in more detail, for example, by combining O_2 imaging with point measurements with O_2 microsensors. Gross photosynthesis rates are normally quantified with fast responding ($t_{90} < 0.2$–0.5 s) O_2 microsensors measuring over <1–2 s intervals after darkening (Kühl et al. 1996). However, our measurements could not realize such high temporal resolution due to limits in the image acquisition system and a relatively slow response of the ~80–100 µm large sensor particles yielding an operational response time of several seconds. Our rates should thus only be regarded as a first proxy of photosynthetic activity in the coral surface tissue. Faster and more precise measurements can, however, be realized with smaller sensor particles, for example, in combination with nano porous polymer matrices facilitating faster

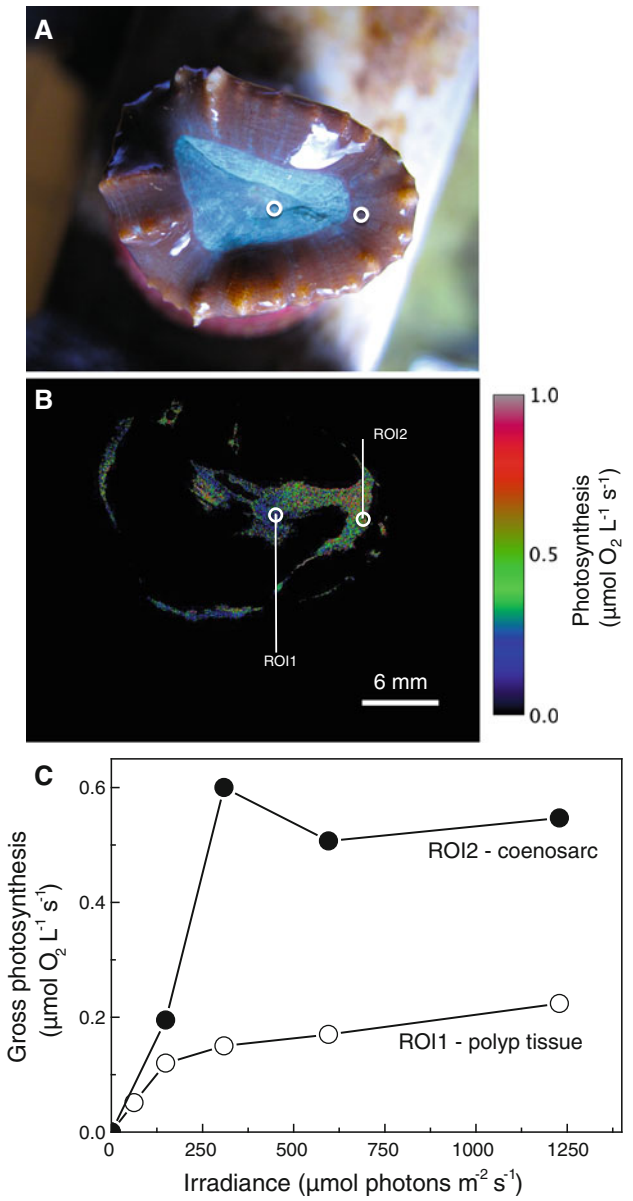

Fig. 7 Imaging of gross photosynthesis rate (GPR) distribution over a single polyp of the coral *Caulastrea furcata*. **a** Digital photo of the coral. **b** Average GPR image measured at an irradiance of 596 µmol photons m^{-2} s^{-1} in polyp tissue (ROI 1) and coenosarcs tissue (ROI 2), respectively. **c** GPR versus irradiance curves calculated as an average of all pixels within ROI 1 (*blue curve*) and ROI 2 (*red curve*)

response times (e.g., Koren et al. 2010). Given sufficient luminescence signal, the imaging system can acquire O_2 images with a time resolution of ~0.5 s (Holst et al. 1998).

During a single acquisition cycle of an O_2 image, light exposure is very brief and does not induce significant O_2 production. However, high frequency image acquisition could potentially induce some photosynthetic activity in dense populated samples with photopigments exhibiting absorption maxima overlapping significantly with the red excitation light. In corals, the main emission of the red LEDs does not directly target photosynthetic pigments of the coral symbionts. This problem may become more severe, for example, in applications with cyanobacteria harboring phycobilins that absorb strongly in the emission range of the red LED. We used the magnetic sensor particles for high frequency measurements in cyanobacterial biofilms and found that the O_2 production rate caused by the LED excitation light used in the luminescent lifetime measurements was <4 % of the maximum production rate (Staal et al. unpublished data). It is important to keep this potential error in mind.

Large particle size makes it difficult to obtain even coverage of areas larger than a few cm^2 without the formation of particle aggregates. Small particle movements, for example due to mucus release or flow variations, can translate into a large standard variation in the measuring signal, especially when doing pixel to pixel calculations as the pixel resolution of the camera system was better than the particle size contributing to noise when one sensor particle is partially monitored by some pixels. These limitations could be alleviated in future studies by using smaller magnetized particles (down to nanoparticle size, Mistlberger et al. 2010a, b).

Another important factor is to provide a strong and homogenous magnetic field in order to facilitate an even and stable distribution of the sensor particles on top of the investigated surface. In this first study, we did not attempt such optimization of the magnetic field besides using strong magnets. However, there is significant know-how developed in analytical chemistry to facilitate such optimization and manipulation of magnetic fields and particles (Mistlberger et al. 2008). Presence of sticky exopolymers or mucus formation at the surface will bind some particles more strongly. However, in the case of corals, mucus production will over time tend to clear the coral tissue surface of remaining sensor particles.

The use of an NIR-emitting O_2 indicator presents several advantages, as it can be excited with low energy red light and emits at >750 nm, which is well outside the range of chlorophyll fluorescence. It is thus possible to map O_2 concentration and dynamics on tissues and biofilms harboring large amounts of photopigment, and to combine such mapping with, for example, mapping of photosynthetic activity via variable chlorophyll fluorescence imaging (Kühl and Polerecky 2008) without interference from the sensor particles. The NIR-emitting O_2 indicator can also be used in combination with other frequently used biomarkers such as green fluorescent protein (GFP) reporters and DNA stains with emission windows outside the range of PtTPTBPF, and this, for example, allows quantification of GFP-like coral host pigments without interference from the sensor particles.

In conclusion, lifetime imaging combined with distributed magnetized optode microparticles can resolve the spatio-temporal dynamics of O_2 over tissue surfaces at a hitherto unreached spatial coverage, allowing images of O_2 concentration and O_2 dynamics to be directly superimposed on structural images of corals. This new methodology is also well suited for studies of O_2 microenvironments at other surfaces with a complex topography, for example, sediments, microbial biofilms, plant and animal tissues. Examples of future applications of such magnetized O_2 sensitive microparticles include, for example, studies of the microenvironment of macrophytes (Spilling et al. 2010) or the epithelia of aquatic organisms that exchange O_2 through their skin rather than via gills. Physiological applications could also encompass the use of metabolic inhibitors and mapping of their spatio-temporal effect on O_2 metabolism. The methodology is also relevant, for example, in studies of DBLs and O_2 dynamics of sediments and solid substrates such as coralline algae (Larkum et al. 2003). Integration of other optical sensor chemistries in the magnetic sensor particles could expand such studies to encompass, for example, measurements of pH (Mistlberger et al. 2010a, b) and temperature (Borisov and Klimant 2008a, b; Borisov et al. 2010) dynamics over complex biotic and abiotic interfaces in the aquatic environment.

Acknowledgments We thank Kristian Vedel and other staff of Øresundsakvariet at the Marine Biology Section for maintenance of the corals and the coral growth facility. Erik Trampe is thanked for help with figure formatting. This study was supported by grants from the Danish Natural Science Research Council (MK) and the Danish Research Council for Technology and Production (MK).

References

Andersen SB, Vestergaard ML, Ainsworth TD, Hoegh-Guldberg O, Kühl M (2010) Acute tissue death (white syndrome) affects the microenvironment of tabular *Acropora* corals. Aquat Biol 10:99–104

Bacon J, Demas J (1987) Determination of oxygen concentrations by luminescence quenching of a polymer-immobilized transition-metal complex. Anal Chem 59:2780–2785

de Beer D, Kühl M, Stambler N, Vaki L (2000) A microsensor study of light enhanced Ca^{2+} uptake and photo-synthesis in the reef-building coral *Favia* sp. Mar Ecol Progr Ser 194:75–85

Behrens JW, Stahl HJ, Steffensen JF, Glud RN (2007) Oxygen dynamics around buried lesser sandeel, *Ammodytes tobiannus* (Linnaeus, 1785); mode of ventilation and metabolic requirements. J Exp Biol 210:1006–1014

Borisov SM, Klimant I (2008a) Blue LED excitable temperature sensors based on a new Europium(III) chelate. J Fluoresc 18: 581–589

Borisov SM, Klimant I (2008b) Luminescent nanobeads for optical sensing and imaging of dissolved oxygen. Microchim Acta 164: 7–15

Borisov SM, Nuss G, Klimant I (2008a) Red light-excitable oxygen sensing materials based on platinum(II) and palladium(II)benzoporphyrins). Anal Chem 80:9435–9442

Borisov SM, Mayr T, Klimant I (2008b) Poly (styrene-block-vinylpyrrolidone) beads as a versatile material for simple fabrication of optical nanosensors. Anal Chem 80:573–582

Borisov SM, Nuss G, Haas W, Saf R, Schmuck M (2009) New NIR-emitting complexes of platinum (II) and palladium (II) with fluorinated benzoporphyrins. J Photochem Photobiol A Chem 201:128–135

Borisov SM, Gatterer K, Bitschnau B, Klimant I (2010) Preparation and characterization of Chromium(III)-activated Yttrium Aluminum Borate: a new thermographic phosphor for optical sensing and imaging at ambient temperatures. J Phys Chem C 114:9118–9124

Carraway ER, Demas JN, DeGraff BA, Bacon JR (1991) Photophysics and photochemistry of oxygen sensors based on luminescent transition-metal complexes. Anal Chem 63:337–342

Cooper TF, Ulstrup KE, Dandan SS, Heyward A, Kühl M, Muirhead A, O'Leary R, Ziersen B, van Oppen MJH (2011) Niche specialisation of reef-building corals in the mesophotic zone: metabolic trade-offs between divergent *Symbiodinium* types. Proc Roy Soc Lond B 278:1840–1850

Dobrucki JW (2001) Interaction of oxygen-sensitive luminescent probes Ru (phen) 32+ and Ru (bipy) 32+ with animal and plant cells in vitro. Mechanism of phototoxicity and conditions for non-invasive oxygen measurements. J Photochem Photobiol B: Biol 65:136–144

Fenchel T, Finlay B (2008) Oxygen and the spatial structure of microbial communities. Biol Rev 83:553–569

Glud RN (2008) Oxygen dynamics in marine sediments. Mar Biol Res 4:243–289

Glud RN, Gundersen JK, Revsbech NP, Jørgensen BB (1995) Effects on the diffusive boundary layer imposed by microelectrodes. Limnol Oceanogr 39:462–467

Glud RN, Ramsing NB, Gundersen JK, Klimant I (1996) Planar optrodes: a new tool for fine scale measurements of two-dimensional O_2 distribution in benthic communities. Mar Ecol Progr Ser 140:217–226

Glud RN, Kühl M, Kohls O, Ramsing NB (1999) Heterogeneity of oxygen production and consumption in a photosynthetic microbial mat as studied by planar optodes. J Phycol 35:270–279

Glud RN, Tengberg A, Kühl M, Hall P, Klimant I, Holst G (2001) An in situ instrument for planar O_2 optode measurements at benthic interfaces. Limnol Oceanogr 46:2073–2080

Holst G, Grunwald B (2001) Luminescence lifetime imaging with transparent oxygen optodes. Sens Act B 74:78–90

Holst G, Kohls O, Klimant I, König B, Richter T, Kühl M (1998) A modular luminescence lifetime imaging system for mapping oxygen distribution. Sens Act B 51:163–170

Jimenez IM, Kühl M, Larkum AWD, Ralph PJ (2008) Heat budget and thermal microenvironment of shallow-water corals: do massive corals get warmer than branching corals? Limnol Oceanogr 53:1548–1561

Jimenez IM, Kühl M, Larkum AWD, Ralph PJ (2011) Effects of flow and colony morphology on the thermal boundary layer of corals. J Roy Soc Interface 8:1785–1795

Klimant I, Kühl M, Glud RN, Holst G (1997) Optical measurement of oxygen and temperature in microscale: strategies and biological applications. Sens Act B 38:29–37

Köhler-Rink S, Kühl M (2005) The chemical microenvironment of the symbiotic planktonic foraminifer *Orbulina universa*. Mar Biol Res 1:68–78

Koren K, Mistlberger G, Aigner D, Borisov SM, Zankel A, Pölt P, Klimant I (2010) Characterization of micrometer-sized magnetic optical sensor particles produced via spray-drying. Monatsh Chem 141:691–697

Kühl M (2005) Optical microsensors for analysis of microbial communities. Meth Enzymol 397:166–199

Kühl M, Polerecky L (2008) Functional and structural imaging of phototrophic microbial communities and symbioses. Aquat Microb Ecol 53:99–118

Kühl M, Cohen Y, Dalsgaard T, Jørgensen BB, Revsbech NP (1995) Microenvironment and photosynthesis of zooxanthellae in scleractinian corals studied with microsensors for O_2, pH and light. Mar Ecol Progr Ser 117:159–172

Kühl M, Glud RN, Ploug H, Ramsing NB (1996) Microenvironmental control of photosynthesis and photosynthesis-coupled respiration in an epilithic cyanobacterial biofilm. J Phycol 32:799–812

Kühl M, Rickelt LF, Thar R (2007) Combined imaging of bacteria and oxygen in biofilms. Appl Environ Microbiol 73:6289–6295

Kühl M, Holst G, Larkum AWD, Ralph PJ (2008) Imaging of oxygen dynamics within the endolithic algal community of the massive coral *Porites lobata*. J Phycol 44:541–550

Larkum AWD, Koch EM, Kühl M (2003) Diffusive boundary layers and photosynthesis of the epilithic algal community of coral reefs. Mar Biol 142:1073–1082

Mistlberger G, Chojnacki P, Klimant I (2008) Magnetic separator with an optical window. J Phys D Appl Phys 41:085003

Mistlberger G, Medina-Castillo AL, Borisov SM, Mayr T, Fernandez-Sanchez JF, Klimant I (2010a) Miniemulsion solvent evaporation: a simple and versatile way to magnetic nanosensors. Mikrochim Acta 172:299–308

Mistlberger G, Koren K, Scheucher E, Aigner D, Borisov SM, Zankel A, Pölt P, Klimant I (2010b) Multi-functional magnetic optical sensor particles with tunable sizes for monitoring metabolic parameters and as basis for nanotherapeutics. Adv Funct Mater 20:1842–1851

Oswald F, Schmitt F, Leutenegger A, Ivanchenko S, D'Angelo C, Salih A, Maslakova S, Bulina M, Schirmbeck R, Nienhaus GU, Matz MV, Wiedenmann J (2007) Contributions of host and symbiont pigments to the coloration of reef corals. FEBS J 274:1102–1109

Ramsing NB, Gundersen JK (2000) Seawater and gases: tabulated physical parameters of interest to people working with microsensors in marine systems. http://www.unisense.com

Revsbech NP (2005) Analysis of microbial communities with electrochemical microsensors and microscale biosensors. Meth Enzymol 397:147–166

Salih A, Larkum AWD, Cox G, Kühl M, Hoegh-Guldberg O (2000) Fluorescent pigments in corals are photoprotective. Nature 408:850–853

Spilling K, Greve TM, Titelman J, Kühl M (2010) Microsensor measurements of the external and internal microenvironment of *Fucus vesiculosus* (Phaeophyceae). J Phycol 46:1350–1355

Staal M, Borisov SM, Rickelt LF, Klimant I, Kühl M (2011) Ultrabright planar optodes for luminescence life-time based microscopic imaging of O_2 dynamics in biofilms. J Microbiol Meth 85:67–74

Ulstrup KE, Ralph PJ, Larkum AWD, Kühl M (2006) Intra-colonial variability in light acclimation of zooxanthellae in coral tissues of *Pocillopora damicornis*. Mar Biol 149:1325–1335

Ulstrup KE, Kühl M, Bourne DG (2007) Zooxanthellae harvested by ciliates associated with brown band syndrome of corals remain photosynthetically competent. Appl Environ Microbiol 73:1968–1975

Weber M, Lott C, Fabricius KE (2006) Sedimentation stress in a scleractinian coral exposed to terrestrial and marine sediments with contrasting physical, organic and geochemical properties. J Exp Mar Biol Ecol 336:18–32

Wenzhöfer F, Glud RN (2004) Small-scale spatial and temporal variability in benthic O_2 dynamics of coastal sediments: Impact of fauna activity. Limnol Oceanogr 49:1471–1481